Optimizing Hyperuniformity in Self-Assembled Bidisperse Emulsions

Joshua Ricouvier,[1,*] Romain Pierrat,[2] Rémi Carminati,[2] Patrick Tabeling,[1] and Pavel Yazhgur[1,†]

[1]*ESPCI Paris, PSL Research University, CNRS, IPGG, MMN, 6 rue Jean Calvin, F-75005 Paris, France*
[2]*ESPCI Paris, PSL Research University, CNRS, Institut Langevin, 1 rue Jussieu, F-75005 Paris, France*

(Received 10 July 2017; published 15 November 2017)

We study long range density fluctuations (hyperuniformity) in two-dimensional jammed packings of bidisperse droplets. Taking advantage of microfluidics, we systematically span a large range of size and concentration ratios of the two droplet populations. We identify various defects increasing long range density fluctuations mainly due to organization of local particle environment. By choosing an appropriate bidispersity, we fabricate materials with a high level of hyperuniformity. Interesting transparency properties of these optimized materials are established based on numerical simulations.

Hyperuniform systems have recently been identified as a particular subclass of disordered systems with density fluctuations vanishing at infinitely large length scales [1]. In Fourier space, the structure factor $S(q)$ reveals hyperuniformity by vanishing when q tends to zero. These systems possess properties of crystals, such as long-range order, in addition to characteristics of disordered systems such as a statistical isotropy. Hyperuniformity has been used as a guideline for creating disordered photonic band gap materials [2–4]. It paves the way for fabricating colloidal materials with forbidden band gaps less sensitive to defects than those observed in ordered colloidal arrangements. Disorder also brings isotropy, useful to create free-form waveguides, laser cavities, noniridescent dyes or display devices [5–7]. It was also shown that hyperuniform materials can be optimized to be optically dense and transparent at the same time [8]. The obtained results have been naturally extended to other types of propagating waves, for example to produce disordered phononic or electronic band gaps [9,10]. Such active hyperuniform materials are now mainly designed on a computer and are printed afterwards [3,4,11,12]. These patterns can be optimized to exhibit a tremendous complete photonic band gap but suffer from severe limitations of 3D printing (time scale, defects, resolution, etc.). By contrast, the bottom-up approach, potentially more interesting in terms of throughput and cost, has not yet led to innovative materials [13,14].

Using numerical simulations, Donev *et al.* predicted [15] that random close packing of spheres can be hyperuniform under certain conditions. Such obtained structures are called maximally random jammed (MRJ) states and are defined as the most disordered strictly jammed packing of solid spheres [16] which minimizes an arbitrary order parameter, e.g., a fraction of crystallized particles. To realize such assemblies, the system should avoid two kinds of defects: rattlers (particles free to move in a confining cage) and crystalline domains. The former refers to zones less dense than the surrounding medium (underpacked

defects), while the latter are denser (overpacked defects) [17]. Both create long range density fluctuations and are unfavorable for hyperuniformity.

In this Letter, we demonstrate the creation of hyperuniform structures by self-assembling bidisperse droplets in a Hele-Shaw configuration using a microfluidic chip. The small friction between liquid droplets, together with deformability, allow us to close the cages around rattling particles and create truly jammed states, while size bidispersity breaks the crystallization. We take advantage of microfluidics to produce a set of particle ensembles in, typically, a few minutes, precisely controlling the size and number ratios of droplets. Thus, we systematically vary both ratios, unlike most studies of jammed states. Interestingly, we discover that hyperuniformity defects can be much more complex than expected. Density fluctuations turn out to be very sensitive to the structure of clusters formed by the particles and their immediate neighbors. Thus, a new approach to describe hyperuniform jammed systems is proposed. We believe that this can guide research for new materials with vanishing density fluctuations.

Our microfluidic device, shown in Fig. 1, is made of standard soft photolithography and replica-molding techniques using polydimethylsiloxane (PDMS). Two populations of droplets (FC-3283 in 0.2% SDS solution) with two different sizes (typically less than 2% of polydispersity) are created in two separate T junctions. The height of the channels (10 μm) forces the droplet to adopt a pancake shape. Therefore, we can consider the system as made of 2D disks which organization does not strongly depend on the true thickness of the Hele-Shaw cell [18]. The droplet size is in the range 20–40 μm. The relatively small size of droplets and high enough surface tension (22 ± 0.5 mN m^{-1}) keep them circular due to Laplace pressure inside while being close to the jamming point. Droplet production rates, and sizes can be tuned by varying pressures in four input channels. As a result, the size ratio (SR) between droplets of different sizes SR $= D_s/D_b$
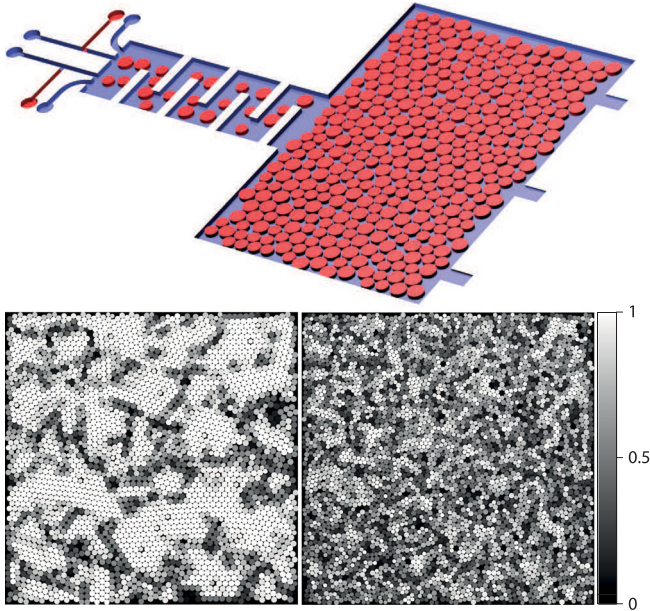
FIG. 1. Top: Scheme of the microfluidic chip. Bottom: Experimental images of droplet assemblies. Gray scale represents the orientational order parameter ψ_6. White particles are crystallized in a hexagonal lattice. SR ≈ 0.8 and NF ≈ 0.88 (left, polycrystal) or NF ≈ 0.38 (right, disordered).

(here, D stands for disk diameters, s for small ones, b for big ones) and the number fraction (NF) of big particles NF $= N_b/N$ are adjustable (N being the number of droplets). Defined this way, both ratios vary from 0 to 1. Then, the droplets pass through the micromixer which brings disorder and homogeneity to the droplets by randomizing their entry in the observation chamber. Upon entering, they self-organize into a close packing by plastic events. Down from the entrance, plastic events rarefy and the droplets seem to adopt their final configuration with almost circular shapes [19]. The ceiling of the observation chamber is reinforced with a glass slide placed inside the PDMS to prevent deformations. Filters are placed downstream to retain droplets inside the cell without stopping fluxes. The filters do not stop the droplets completely but let them pass slowly, allowing one to renew the packing continuously. Top view microscopy images of $N \simeq 3000$ particles can be taken allowing one to probe wave vectors as small as $q_{\min} \sim 1/(D_m \sqrt{N})$, D_m being the mean diameter of disks. To avoid any ordering due to the walls, deformation close to the filters at the exit, and loosely packed zones at the entrance, the pictures are taken at least five layers away from the edges of the observation chamber [19,20]. The interval between images is typically on the order of 30 seconds, which corresponds to the duration of the filling of the observation chamber. Therefore, systems are completely refreshed, and the images are uncorrelated. For each experimental set of parameters, at least 30 images are taken. Statistical measures (e.g., structure factor, fraction of particles with a given coordination) are calculated on each image and then averaged over the full ensemble. In each experimental set we have checked that the populations are well mixed and no global gradients of small or big particle concentrations are present. We also ensure isotropy of images by checking circular symmetry of their Fourier transforms.

We also perform numerical simulations of 2D bidisperse jammed assemblies of disks using freely available code based on the Lubachevsky-Stillinger algorithm. It is based on a collision-driven packing generation, and is shown to create a highly jammed bidisperse assembly of disks with a low rate of rattlers [21,22].

To explore the whole diagram of different size ratios and number fractions, we start by keeping the size ratio SR constant, at a value 0.8 which is a standard value used in most previous studies [23,24], and varying NF. We observe that for values of NF close to 0 or 1, the system forms a polycrystal with well distinguishable hexagonal crystal domains. For moderate NF values, we observe disordered structures where crystal domains are small and rare, and the assembly resembles a homogeneous mixture of small and big disks. Two experimental pictures for both polycrystal and disordered systems are shown in Fig. 1. To be more quantitative, the experimental pictures are colored using the bond orientational order parameter ψ_6, which shows how the weighted Voronoi cell for each particle is close to a regular hexagon and gives it a score from 0 to 1, approaching 1 for particles with an ideal sixfold symmetry. By considering a particle to be crystallized if $\psi_6 > 0.9$, we plot, in Fig. 2(a), the fraction of crystallized particles both for experimental and simulated samples as a function of NF. The data clearly show that there exists an optimum where the fraction of crystallized particles is minimized. It is close to this point that MRJ and the most hyperuniform systems are expected. Figure 2(a) also shows that the rate of rattlers, defined as particles having less than three neighbor contacts, is always rather low in our system (less than 1%). Therefore, they should not strongly affect the structural properties. This also indicates that we, indeed, succeed in approaching a jamming point.

To check hyperuniformity of the obtained samples, we calculate the spectral density $\chi(\mathbf{q})$, which is an extension of the classical structure factor for bidisperse and, more generally, polydisperse particle assemblies. In our calculations, we use the spectral density definition which treats each particle as a point object with weight equal to the particle area [25,26]

$$\chi(\mathbf{q}) = \frac{1}{N\langle s_i^2 \rangle} |\phi(\mathbf{q})|^2, \tag{1}$$

where N is the number of particles and s_i are their areas. In this expression, $\phi(\mathbf{q})$ is the Fourier transform of the surface fraction defined as
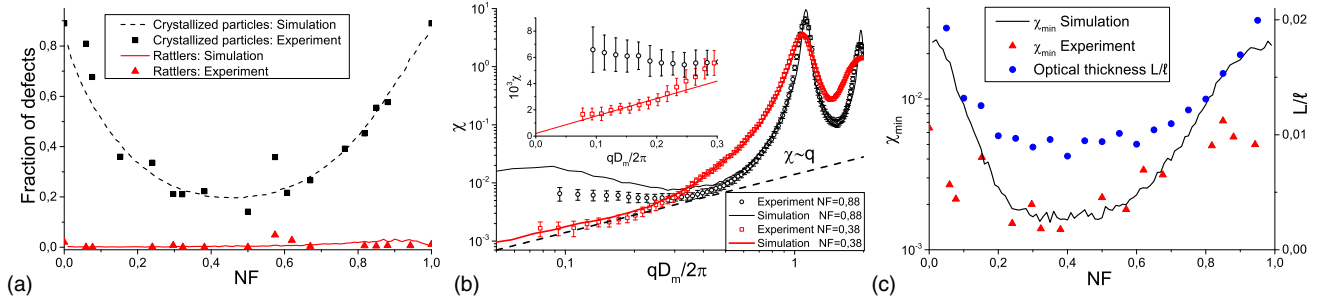
FIG. 2. (a) Fraction of crystalline particles and rattlers for simulated and experimental binary mixtures of solid particles for different fraction of big ones NF. (b) Spectral density of a binary disk mixture for different fractions of big particles NF. Linear dependence $\chi \sim q$ characteristic of MRJ systems is shown as a guide for eyes. Inset: linear fit of experimental data for NF ≈ 0.38, y intercept $(2 \pm 3) \times 10^{-4}$. (c) Spectral density at minimum experimentally available wave vector ($qD_m/2\pi \approx 0.1$) and optical thickness of the simulated 2D jammed assemblies L/ℓ as a function of NF. The refractive index is 1 for the host medium and 1.3 for the droplets. A strong correlation between the fraction of crystal particles, the minimum spectral density $\chi_{\min}$ and optical thickness L/ℓ is clearly observed. All figures correspond to SR ≈ 0.80.

$$\phi(\mathbf{r}) = \sum_i s_i \delta(\mathbf{r} - \mathbf{r}_i), \qquad (2)$$

where $\mathbf{r}_i$ are the positions of individual particle centers.

Figure 2(b) shows two spectral densities $\chi(\mathbf{q})$ in the polycrystal and disordered cases (SR ≈ 0.8). The spectral density of a polycrystalline system is not hyperuniform. Indeed, $\chi(\mathbf{q})$ does not monotonically decrease while approaching zero but, rather, passes through a local maximum. The latter can be related to the size and distance between the crystal domains. On the contrary, for disordered systems close to the minimum of crystallized particle fractions, the spectral density approaches a linear behavior as predicted for MRJ [see Fig. 2(b)] [15]. A linear fit shown in the inset reveals a very low spectral density limit $\chi(q=0) = (2 \pm 3) \times 10^{-4}$. This confirms hyperuniformity of our optimized systems [26,27].

Strictly speaking, hyperuniformity is defined only at infinite length scales, which are not relevant for real materials nor accessible experimentally [14,27]. To estimate the degree of hyperuniformity in the finite system, we choose the spectral density $\chi_{\min}$ at the minimum wave vector ($qD_m/2\pi \approx 0.1$) available from our experimental data. It probes density fluctuations at large length scale about ten particle diameters which are sufficient for the sought optical properties [28]. Also, compared to the y intercept, $\chi_{\min}$ does not assume any linear behavior which is, for instance, disputed in [29]. Both experiments and simulations reveal that $\chi_{\min}$ has a single minimum at NF ≈ 0.3–0.4 [Fig. 2(c)] similar to the previously described ψ_6. This result proves the dominating role of crystalline domains in the behavior of the spectral density, and guides us towards the most hyperuniform systems available experimentally for a given SR.

We also use numerical simulations of light scattering to demonstrate that the optimized bidisperse emulsions are good candidates for the production of high-density and transparent disordered materials. In order to explore a range

of scattering wave vectors q minimizing the structure factor, we have chosen $\lambda = 500~\mu m$ which corresponds to $k_0 D_m/(2\pi) = 0.12$, so that $|q| \sim k_0$ lies in the region where the spectral density takes very small values. Light scattering from the numerically generated 2D jammed assemblies (TE polarization, electric field perpendicular to the plane) is simulated by solving Maxwell's equations using the coupled-dipoles method [30]. We use the Mie theory to compute the scattering cross sections σ_s of a single disk, and replace each disk by an electric point dipole with an effective polarizability giving the same scattering cross section as the real droplet. From the calculation of the average field inside the medium, we deduce the real scattering optical thickness L/ℓ of the structures, where L is the sample thickness and ℓ the scattering mean free path [31]. In Fig. 2(c), we observe that scattering is strongly suppressed for samples exhibiting the highest degree of hyperuniformity. This analysis supports that the microfluidic fabrication technique described in this Letter is an important step towards the assembly of hyperuniform materials for photonics.

Interestingly, we can also remark that, while the concentration of crystallized particles is similar for experimental and simulated systems [Fig. 2(a)], considering $\chi_{\min}$, there exists a small discrepancy for polycrystalline samples [Fig. 2(c)]. The latter is affected not only by the fraction of crystallized particles, but also by the size and shape of crystal domains, which are rather sensitive to the generation process. In the meantime, production of hyperuniform systems is much more robust, making them even more attractive for potential applications.

Surprisingly, we cannot simply extend this correlation between $\chi_{\min}$ and ψ_6 for systems with various size ratios. Actually, by varying the size ratio for a fixed number fraction NF ≈ 0.5, we reveal the existence of a few local minima for $\chi_{\min}$, pointing out a much more complex behavior [see Fig. 3(a)]. Several size ratios, ranging from 0.3 to 0.8 seem to have a low rate of density fluctuations.
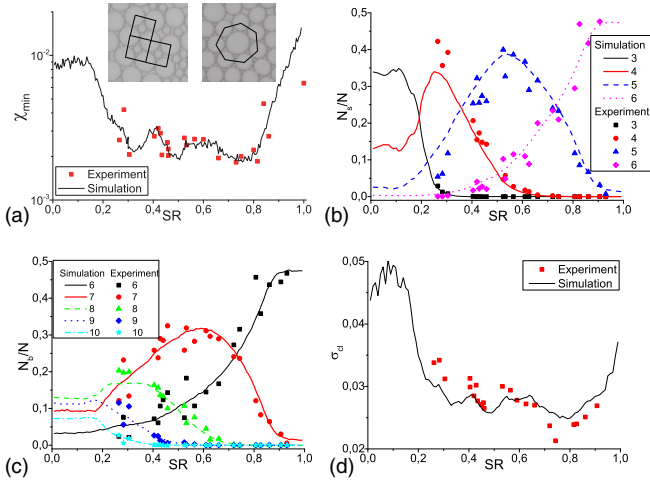
(a)

(b)

(c)

(d)

FIG. 3. (a) Spectral density $\chi_{\min}$ at minimum experimentally available wave vector ($qD_m/2\pi \approx 0.1$). Peaks and valleys are signatures of complex internal organization of different defects. Two examples of overpacked defects: a bidisperse crystal domain with fourfold symmetry SR $\approx$ 0.40 (left), a cluster of a big particle surrounded by seven small particles SR $\approx$ 0.70 (right). (b) Fraction of small particles having a given coordination number as a function of SR. (c) Fraction of big particle having a given coordination number as a function of SR. (d) Variance for cluster local fraction. All figures correspond to NF $\approx$ 0.50.

The crystallization can still account for the general behavior of the system, namely for the increase of density fluctuations for SR close to 0 and 1. But, peaks and valleys for $\chi_{\min}$ for medium range of SR (0.3–0.8) cannot be explained solely with the hexagonal crystal domains, and thus, second order defects should be introduced. A similar nonmonotonic behavior has been previously described for the surface fraction of simulated bidisperse jammed assemblies, although no explanation has, so far, been provided [32,33].

The initial reduction of density fluctuations with decreasing SR from 1 is explained by the destruction of hexagonal crystal zones by analogy with NF varying systems. The minimum spectral density $\chi_{\min}$ reaches its extremum about SR $\approx$ 0.8. As shown in Figs. 3(b) and 3(c), for size ratio below 0.8, small particles with coordination five (number of edges of their weighted Voronoi cell) and big particles with coordination seven can be identified [33]. The particles under consideration, together with their closest neighbors, can arrange in compact clusters at appropriate size ratios. Actually, the first type of such clusters is a big particle surrounded by seven small ones [see Fig. 3(a)]. From simple geometrical considerations, we can predict the size ratio SR where these clusters appear by calculating the ideal cluster conformation: $\sin(\pi/7)/[1-\sin(\pi/7)] \approx 0.76$. To give a quantitative estimate of the cluster density, we define, for each particle, the cluster fraction φ_{cl}^{i} as the ratio of the occupied surface in the polygon, whose vertices are the centers of the surrounding particles, over its area A_i (Fig. 4). For instance, in the considered example, we find a

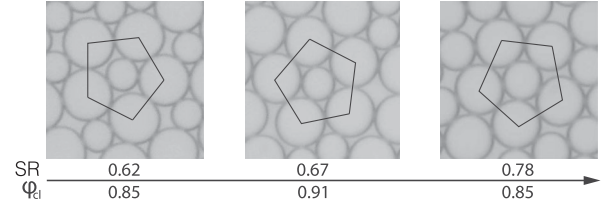| SR | 0.62 | 0.67 | 0.78 |
| φ_{cl} | 0.85 | 0.91 | 0.85 |

FIG. 4. Geometrical resonance for a cluster of one small and five big particles. Three size ratios are shown: slightly before, close, and slightly after the resonance size ratio SR $\approx$ 0.7 corresponding to a compact cluster. The compact cluster has a density φ_{cl} well above the loosely packed ones.

cluster fraction on the order of 0.909, slightly higher than that corresponding to hexagonal crystals (0.906) and much higher than the average surface fraction (about 0.84). Such clusters are geometrical defects that locally increase the density and create additional fluctuations.

Each type of cluster is compact only at a particular size ratio SR, and exists mainly in the vicinity of this SR. Typically, below and above the characteristic size, the clusters are loosely packed and have a density comparable to the surrounding medium, while close to the characteristic SR they form overpacked defects (see Fig. 4). This gives a kind of geometric resonance for the spectral density. In the range of SR about 0.5–0.7, a rich morphology of clusters exists with coordination five and seven for the central particle. For example, we can identify small particles surrounded by two big and three small particles, or by three big and two small particles, etc. In this Letter, we do not intend to precisely describe the whole variety, although a tentative classification has been proposed [34]. Resonances for different cluster types overlap, giving a plateau of $\chi_{\min}$. In comparison to hexagonal crystal domains, these overpacked defects do not have large spatial extensions and are often limited to one cluster, thus, creating only second order fluctuations.

In Fig. 3(a), the peak around SR $\approx$ 0.4 is particular as it is due to the appearance of fourfold symmetry bidisperse crystal domains. The footprints of this crystal are found in the increased fraction of small particles with coordination four, and of big particles with coordination eight [see Figs. 3(b) and 3(c)]. A peculiarity of these clusters is that they are often organized in small crystallized zones [Fig. 3(a)]. As hexagonal crystal zones, such domains have higher density and, therefore, increase the density fluctuations. They are overpacked defects that often extend to more than one cluster. Actually, in a first approximation (low rate of defects), we can estimate that the influence of any defect on $\chi_{\min}$ scales with its concentration and the surface area square. This power law suggests that even small crystal zones influence the spectral density much more than the individual clusters. Also, other types of bidisperse crystal domains are expected to appear (see Refs. [34,35] for some examples).

If SR decreases further, the fourfold crystals start to be mechanically unstable, and below SR $\approx$ 0.15, they are

replaced by Appolonian packing (small particles in the interstices between three big ones). This packing is clearly observed by the appearance of a coordination three for small particles and larger than nine for big particles. The big particles are organized in hexagonal crystal domains which then cause large increase of $\chi_{\min}$. Some additional density fluctuations may arise due to the fact that small particles may occupy only a part of interstices. These small particles in the interstices also show an example of rattlers (particles with less than three neighboring contacts) which can be overpacked defects or even have a cluster fraction close to the mean value. Hence, we prefer to describe the system in terms of overpacked and underpacked defects.

In order to properly monitor the quantity of various clusters, we can calculate for the set of obtained cluster local fractions φ_{cl}^i the standard deviation σ_{cl} weighted by the cluster area $A_i / \sum A_i$. The evolution of this quantity versus the size ratio is presented in Fig. 3(d) for NF ≈ 0.5, showing that we are able to recover all peaks and valleys given by $\chi_{\min}$. The standard deviation σ_{cl} reports local phenomenon by measuring the disparity of every cluster towards the mean surface fraction of the system, and, $\chi_{\min}$ reports density fluctuations at large length scale. Therefore, for jammed particle assemblies, we can correlate hyperuniformity at large length scales and the local environment of particles. It also makes σ_{cl} a useful tool for estimating density fluctuations with finite size images. The fact that hyperuniformity is related to local particle environment also gives expectations to make a statistical description of the problem using a kind of granocentric model such as in Refs. [36,37].

To conclude, we have successfully produced large sets of two dimensional bidisperse jammed assemblies with well controlled size and number ratios. In an optimized range of parameters, structures with reduced large scale density fluctuations, or equivalently, a high level of hyperuniformity, emerge. Thus, this work confirms the relevance of microfluidics for the rapid production of large scale self-assembling hyperuniform materials [13]. The geometrical features of the fabricated structures are supported by numerical simulations, in very good agreement with the experiments. Our results establish links between the overall local parameters such as coordination and cluster fraction, and long range density fluctuations. This can potentially help to suggest hyperuniformity for a much wider range of systems incompatible with long range analysis. The proposed experimental approach also has the potential to be extended to study 3D packings [36,37] and could lead to the fabrication of optically dense and transparent materials, as suggested by light scattering simulations.

J. R. and P. Y. contributed equally to this work.

---

*Corresponding author.
joshua.ricouvier@espci.fr
†Corresponding author.
pavel.yazhgur@unifr.ch

[1] S. Torquato and F. H. Stillinger, Phys. Rev. E **68**, 041113 (2003).

[2] M. Florescu, S. Torquato, and P. J. Steinhardt, Proc. Natl. Acad. Sci. U. S. A. **106**, 20658 (2009).

[3] N. Muller, J. Haberko, C. Marichy, and F. Scheffold, Adv. Opt. Mater. **2**, 115 (2014).

[4] N. Muller, J. Haberko, C. Marichy, and F. Scheffold, Optica **4**, 361 (2017).

[5] W. Man, M. Florescu, E. P. Williamson, Y. He, S. R. Hashemizad, B. Y. Leung, D. R. Liner, S. Torquato, P. M. Chaikin, and P. J. Steinhardt, Proc. Natl. Acad. Sci. U.S.A. **110**, 15886 (2013).

[6] J.-G. Park, S.-H. Kim, S. Magkiriadou, T. M. Choi, Y.-S. Kim, and V. N. Manoharan, Angew. Chem., Int. Ed. Engl. **53**, 2899 (2014).

[7] R. Degl'Innocenti, Y. Shah, L. Masini, A. Ronzani, A. Pitanti, Y. Ren, D. Jessop, A. Tredicucci, H. Beere, and D. Ritchie, Sci. Rep. **6**, 19325 (2016).

[8] O. Leseur, R. Pierrat, and R. Carminati, Optica **3**, 763 (2016).

[9] G. Gkantzounis, T. Amoah, and M. Florescu, Phys. Rev. B **95**, 094120 (2017).

[10] M. Hejna, P. J. Steinhardt, and S. Torquato, Phys. Rev. B **87**, 245204 (2013).

[11] W. Man, M. Florescu, K. Matsuyama, P. Yadak, G. Nahal, S. Hashemizad, E. Williamson, P. Steinhardt, S. Torquato, and P. Chaikin, Opt. Express **21**, 19972 (2013).

[12] J. Haberko and F. Scheffold, Opt. Express **21**, 1057 (2013).

[13] J. H. Weijs, R. Jeanneret, R. Dreyfus, and D. Bartolo, Phys. Rev. Lett. **115**, 108301 1 (2015).

[14] R. Dreyfus, Y. Xu, T. Still, L. A. Hough, A. G. Yodh, and S. Torquato, Phys. Rev. E **91**, 012302 (2015).

[15] A. Donev, F. H. Stillinger, and S. Torquato, Phys. Rev. Lett. **95**, 090604 (2005).

[16] S. Torquato, T. M. Truskett, and P. G. Debenedetti, Phys. Rev. Lett. **84**, 2064 (2000).

[17] J. M. Rieser, C. P. Goodrich, A. J. Liu, and D. J. Durian, Phys. Rev. Lett. **116**, 088001 (2016).

[18] K. W. Desmond, P. J. Young, D. Chen, and E. R. Weeks, Soft Matter **9**, 3424 (2013).

[19] D. Chen, K. W. Desmond, and E. R. Weeks, Phys. Rev. E **91**, 062306 (2015).

[20] K. W. Desmond and E. R. Weeks, Phys. Rev. E **80**, 051305 (2009).

[21] M. Skoge, A. Donev, F. H. Stillinger, and S. Torquato, Phys. Rev. E **74**, 041127 (2006).

[22] S. Atkinson, F. H. Stillinger, and S. Torquato, Phys. Rev. E **94**, 032902 (2016).

[23] A. Donev, F. H. Stillinger, and S. Torquato, Phys. Rev. Lett. **96**, 225502 (2006).

[24] C. E. Zachary, Y. Jiao, and S. Torquato, Phys. Rev. Lett. **106**, 178001 (2011).

[25] Y. Wu, P. Olsson, and S. Teitel, Phys. Rev. E **92**, 052206 (2015).

[26] L. Berthier, P. Chaudhuri, C. Coulais, O. Dauchot, and P. Sollich, Phys. Rev. Lett. **106**, 120601 (2011).

[27] R. Kurita and E. R. Weeks, Phys. Rev. E **84**, 030401 (2011).

[28] L. S. Froufe-Pérez, M. Engel, P. F. Damasceno, N. Muller, J. Haberko, S. C. Glotzer, and F. Scheffold, Phys. Rev. Lett. **117**, 053902 (2016).

[29] A. Ikeda, L. Berthier, and G. Parisi, Phys. Rev. E **95**, 052125 (2017).

[30] M. Lax, Phys. Rev. **85**, 621 (1952).

[31] See Supplemental Material at http://link.aps.org/supplemental/10.1103/PhysRevLett.119.208001 for the detailed description of electromagnetic simulations.

[32] D. Koeze, D. Vågberg, B. Tjoa, and B. Tighe, Europhys. Lett. **113**, 54001 (2016).

[33] A. Mascioli, C. J. Burke, M. Q. Giso, and T. Atherton, Soft Matter **13**, 7090 (2017).

[34] T. Kennedy, Discrete Comput. Geom. **35**, 255 (2006).

[35] A. Heppes, Discrete Comput. Geom. **30**, 241 (2003).

[36] M. Clusel, E. I. Corwin, A. O. Siemens, and J. Brujić, Nature (London) **460**, 611 (2009).

[37] I. Jorjadze, L.-L. Pontani, K. A. Newhall, and J. Brujić, Proc. Natl. Acad. Sci. U.S.A. **108**, 4286 (2011).